Composites Part B: Engineering, Volume 199, October 2020, Article number 108288
10.1016/j.compositesb.2020.108288

Numerical Analysis and Experiment of Sandwich T-joint Structure Reinforced by Composite Fasteners

Shijun Guo, Wenhao Li *

Centre of Aeronautics, School of Aerospace, Transport and Manufacturing, Cranfield University, Cranfield, MK43 0AL, UK

Abstract

This study presents an investigation into the failure mechanism and strength improvement of a sandwich composite T-joint bonded and reinforced by fasteners made of thermal plastic composite. The T-joint subjected to pulling load was analysed by numerical simulation and experiment methods. Cohesive zone model (CZM) and Hashin damage criteria were used in the FE analysis to simulate the crack propagation. According to the results, the composite joint reinforcement is mainly attributed to the resistance of composite fasteners to shear failure of the bonded interface. Following the interface delamination and crack propagation in mode II failure, fracture of the composite fasteners occurred in transverse shear mode. The results show nearly 19% increase of bonding strength for the T-joint reinforced by composite fasteners of 5mm diameter compared to the T-joint without fasteners. After the interface delamination, pull-out failure of fasteners was also observed and correlated to the numerical model considering material property reduction due to the sparse fibre tows in the fastener head forming and T-joint assembly. The investigation was extended to a parametric study of diameter and fibre orientation of the composite fasteners. The results show that the T-joint reinforced by composite fasteners of 6.28 mm diameter and $[(\pm 35)_4]_s$ lay-up can achieve the same strength and 44% weight saving compared to a titanium fastener opponent of 5mm diameter.

Keywords: A. sandwich composite T-joint, B. composite fastener, D. mechanical testing, E. failure mechanism.

---

*Corresponding author

Email: wenhao.li@cranfield.ac.uk

1. Introduction

The employment of carbon/epoxy composite in large civil airframe structures is fast growing in the last decade. The trend has raised increasing interest in technology development to improve the structural efficiency subject to integrity. While T-shape joint is the most common type of structure as the result of airframe assemblies such as the connection of skin cover with spars and ribs and fuselage frames. In the manufacturing process, the composite structures are either co-cured or co-bonded along the joints of the components. Since the joints are vulnerable to delamination especially in the joints such as web/flange junctions due to load transfer demand [1], [2], and therefore traditional riveting and bolting techniques have been extensively adopted for the bonded T-joint structures to ensure structural integrity and meet airworthiness requirements. It also offers an additional safeguard to take into account the lack of ductile mechanical behaviour and prevent catastrophic failure of bonded composite joints under excessive load. Although a variety of research has been developed to study the failure mechanism of bonded and bonded/bolted single-lap joints [3]–[8], the study of T-joint conducted so far has mainly focused on the adhesively bonded type [9]–[11] and the study into bonded/bolted T-joints is limited [12].

However, another issue raised by extensive use of metallic fasteners is the weight and expenses penalties [13], [14]. Besides, when metallic fastener in contact with the composite structure, galvanic corrosion arises which significantly reduce the durability of the structure[15], [16]. A composite fastener has been proposed as an alternative to the metallic fastener in the current study to overcome the overweight and corrosion problems. The available information on this rather new and novel area of research is limited at the moment [17]–[20]. Starikov and Schön have experimentally investigated the quasi-static and fatigue behaviour of composite joints with countersunk composite and metallic fasteners [17], [18]. Masahito Ueda at al [19] presented a study on using thermoplastic composite fastener to reinforce composite laminates. The bolted single-lap joint was tested under tension, and compared with that reinforced by metal. The experimental results showed that the strength of the joints increased with the increase of the fibre volume fraction. The joints reinforced by composite fastener yields great weight reduction in comparison to that reinforced by metal. Recently, Li et al [20] experimentally and numerically investigated the benefits arising from using composite reinforcement on bonded single-lap joints.

The herein referenced research publications [17]–[19] relied on time-consuming and expensive experimental approaches. Therefore, one of the objectives was, apart from experimentally testing the T-joint reinforced by composite fasteners, to validate and predict the failure behaviour of such structures. In this regard, damage model has been proposed which can provide a full of perceptive insights into the behaviour of structure in particularly of failure mechanism [21]–[23]. Camanho and Matthews [24] presented a continuum damage model for mechanically fastened joints. Their three-dimensional finite element model implemented with Hashin three-dimensional failure criterion were coupled with internal state variables that apply degradation factors to material elastic properties for joint failure prediction. Zhou et al. [25] developed a continuum damage model on a plain weave two-dimensional composite with Hashin damage criterion having been used to indicate the damage initiation and an Abaqus user subroutine UMAT to modify the stiffness degradation of the material. Hu et al. [26] presented a continuum damage model for simulating bolted single-lap joints for the entire damage process, and cohesive elements inserted are responsible for predicting delamination. M. Tarfaoui et al. [27] investigated the FE model of the composite laminate containing carbon nanotubes using Hashin damage criterion and cohesive elements. The effect of initial crack on the ultimate strength of adhesive joint was reported by Francesco Ascione [28] based on an interface cohesive model. Cui Hao et al. [29] developed an FE model of adhesively bonded composite T-joints under a pulling load to predict the random crack in filling zone. An improved cohesive law with different modifications proposed by Cui Hao [30] provided good prediction of ductile adhesive failure simulation for mixed-mode fracture. Francesco Ascione [31] developed a simple and effective iterative procedure to disregard the mutual effects between normal and tangential stress at adhesive interface, which successfully addressed the equilibrium problem in a FRP lap-joint.

A large amount of work has been carried out in previous research to predict the strength of composite joints of pure bonding or reinforced by metallic fasteners. However few efforts have been paid to composite fasteners for joint reinforcement. The present study is to reveal the failure mechanism of a sandwich composite T-joint with composite fastener reinforcement by numerical simulation and validated by experiment. The T-joint structure was modelled by using FEM in the usual approach. The composite fastener was modelled by using 3D solid elements along with cohesive elements for the adhesive layer between the plies. This model provides the base to obtain insight of the progressive failure of the T-joint with the composite fasteners playing the role of joint strength enhancement and crack arresting. Compared with the

conventional metallic fasteners, the fasteners made of thermal plastic composite materials provide an alternative of great potentials in weight saving, equivalent joint reinforcement and a similar process for composite structure assembly.

2. The T-Joint Model and Experimental Set-up

2.1 The sandwich T-joint sample

The manufacturing process of the T-joint test samples used in this study is the same as that presented in previous research [1]. The composite T-joint was made of sandwich web and base panels bonded in right angle using composite cleats of L-shape with geometry details shown in Figure1. Both base and web panels were made of 5 mm foam core with composite faces bonded on both sides. The web panel face sheet of 1 mm thickness was made of four plies of carbon-epoxy prepreg (MTM46/HTS) in a symmetric layup $[\pm 45]_s$. The foam core along the upper edge of the web panel was replaced by solid laminate to form a monolithic composite part as shown in Figure 1 (a). The base panel face sheet of 2 mm thickness was made of eight plies of the same material in a symmetric layup $[\pm 45/0/90]_s$. For assembly purpose, the foam core in the central part of the base panel was removed and the upper face was dropped and connected with the lower face to form a monolithic laminate as shown in Figure 1. The L-shape cleats of 2 mm thickness made of plain wave cloths were bonded to both sides of the two panels in the joint region. The triangle gap between the panels and cleats in the joint region was filled with adhesive to form an adhesively bonded composite T-joint sample. For the test sample reinforced by fasteners, three holes of 5 mm diameter were drilled through the cleats and base panel on each side of the web panel. To clamp the T-joint sample and apply load for the experiment, holes were drilled along the edges of the web panel and base panel as illustrated in Figure 1 (b).

2.2 Composite fastener manufacture

The manufacturing process of composite fasteners made of thermal plastic composite (PEEK) is divided into two stages: manufacture of composite rod and forming of fastener head and tail when installing the fastener to the T-joint, as shown in Figure 2 (a). To form the rod, 12 plies pre-cut carbon-epoxy (MTM46/HTS) prepreg of 0.16 mm thickness was rolled tightly to form a solid rod with fibres oriented in longitudinal direction. The composite rod of 5 mm diameter and 13 mm length was compressed and autoclaved in a steel mould. In assembly, the composite fastener was inserted into the T-joint reinforcement hole of 7 mm depth with 3 mm length of

the rod on each side left outside of the hole. To form the rivet head and tail, a specially made mould together with a soldering iron was used to deform the pultruded head by applying pressure and temperature in 200°C for 20 minutes to the head as shown in Figure 2 (b). The deformed head together with the forming jig were then pressed by a constant load until cooling down to room temperature. Figure 2 (c) shows a few samples of the cured composite rods of varied length and diameter with formed fastener head. The same process was applied to forming the rivet tail at the other end of the rivet. The assembled composite fastener is shown in Figure 2 (d). Three T-joint test samples were manufactured for test in the study.

2.3 The T-joint experiment set-up

To conduct the experiment, the base panel of the sandwich T-joint was bolted to T-shape test rig made of steel; the top of web panel was bolted to couple of steel flat panels as shown in Figure 3. The test rigs were mounted to the loading head of a test machine through a lug as shown in Figure 3. The pulling load was applied to the T-joint through the web penal until failure occurs in the T-joint samples.

3. Progressive Damage model

3.1 Progressive damage model of composite fasteners

3.1.1 3D material damage model

For composite fasteners that can accumulate damage before fastener collapse, a fibre and matrix damage variable was adopted into the stress-strain constitutive relation to sustain progressive damage through degradation of material stiffness. The continuum damage model (CMD) from [32], [33] employed in this study can be written as follow.

$$\begin{bmatrix}\sigma_{11}\\ \sigma_{22}\\ \sigma_{33}\\ \sigma_{12}\\ \sigma_{23}\\ \sigma_{31}\end{bmatrix}=\begin{bmatrix}(1-d_f)C_{11} & (1-d_f)(1-d_m)C_{12} & (1-d_f)C_{13} & 0 & 0 & 0\\ (1-d_f)(1-d_m)C_{12} & (1-d_m)C_{22} & (1-d_m)C_{23} & 0 & 0 & 0\\ (1-d_f)C_{13} & (1-d_m)C_{23} & C_{33} & 0 & 0 & 0\\ 0 & 0 & 0 & 2(1-d_f)(1-d_m)G_{12} & 0 & 0\\ 0 & 0 & 0 & 0 & 2(1-d_m)G_{23} & 0\\ 0 & 0 & 0 & 0 & 0 & 2(1-d_f)G_{31}\end{bmatrix}\begin{bmatrix}\varepsilon_{11}\\ \varepsilon_{22}\\ \varepsilon_{33}\\ \varepsilon_{12}\\ \varepsilon_{23}\\ \varepsilon_{31}\end{bmatrix} \quad (1)$$

$$d_m = 1-(1-d_{mt})(1-d_{mc}) \quad (2)$$

$$d_f = 1-(1-d_{ft})(1-d_{fc}) \quad (3)$$

$$C_{11} = E_{11}(1 - \nu_{23}\nu_{32})\Delta \tag{4}$$

$$C_{22} = E_{22}(1 - \nu_{13}\nu_{31})\Delta \tag{5}$$

$$C_{33} = E_{33}(1 - \nu_{12}\nu_{21})\Delta \tag{6}$$

$$C_{12} = E_{11}(\nu_{21} + \nu_{31}\nu_{23})\Delta \tag{7}$$

$$C_{23} = E_{22}(\nu_{32} + \nu_{12}\nu_{31})\Delta \tag{8}$$

$$C_{13} = E_{11}(\nu_{31} + \nu_{21}\nu_{32})\Delta \tag{9}$$

$$\Delta = 1/(1 - \nu_{12}\nu_{21} - \nu_{23}\nu_{32} - \nu_{13}\nu_{31} - 2\nu_{21}\nu_{32}\nu_{13}) \tag{10}$$

Where C_{ij} is the material stiffness tensor, damage variables d_i $(i = m\ and\ f)$ are the damage state of matrix and fibre varying from 0 to 1, associated with the tension $(d_{mt}\ and\ d_{ft})$ and compression $(d_{mc}\ and\ d_{fc})$ damage respectively.

3.1.2 Damage Initiation

Three-dimensional Hashin failure criterion [34] was adopted for composite fastener model to better account for composite fastener damage initiation under complex 3D stress level by taking the out-of-plane stress into consideration. The 3D Hashin damage failure criterion taking into account of four damages: fibre tension failure, fibre compression failure, matrix tension failure and matrix compression failure, as presented below in general forms:

Fibre failure in tension ($\sigma_{11} \geq 0$):

$$F_{ft} = (\frac{\sigma_{11}}{X_t})^2 + \frac{\sigma_{12}^2 + \sigma_{13}^2}{{S_{12}}^2} = \begin{cases} \geq 1 & \text{failure} \\ < 1 & \text{no failure} \end{cases} \tag{11}$$

Fibre failure in compression ($\sigma_{11} < 0$):

$$F_{fc} = (\frac{\sigma_{11}}{X_c})^2 = \begin{cases} \geq 1 & \text{failure} \\ < 1 & \text{no failure} \end{cases} \tag{12}$$

Matrix cracking failure in tension ($\sigma_{22} + \sigma_{33} \geq 0$):

$$F_{mt} = \left(\frac{\sigma_{22} + \sigma_{33}}{Y_t}\right)^2 + \frac{\sigma_{23}^2 - \sigma_{22}\sigma_{33}}{{S_{23}}^2} + \frac{\sigma_{12}^2 + \sigma_{13}^2}{{S_{12}}^2} = \begin{cases} \geq 1 & \text{failure} \\ < 1 & \text{no failure} \end{cases} \quad (13)$$

Matrix cracking failure in compression ($\sigma_{22} + \sigma_{33} < 0$):

$$F_{mc} = \left[\left(\frac{Y_c}{2S_{23}}\right)^2 - 1\right]\left(\frac{\sigma_{22} + \sigma_{33}}{Y_c}\right) + \frac{(\sigma_{22} + \sigma_{33})^2}{4{S_{23}}^2} + \frac{\sigma_{23}^2 - \sigma_{22}\sigma_{33}}{S_{23}^2} + \frac{\sigma_{12}^2 - \sigma_{13}^2}{S_{12}^2} = \begin{cases} \geq 1 & \text{failure} \\ < 1 & \text{no failure} \end{cases} \quad (14)$$

Where σ_{ij} are the components of the effective stress tensor, X_t and X_c are the tensile and compressive strength in the longitudinal direction, Y_t and Y_c are the tensile and compressive strength in the transverse direction, S_{12} , S_{23} and S_{13} are the in-plane and out-of-plane shear strengths respectively.

3.1.3 Damage Evolution

After failure predicted using the above criterion, in this paper a stress-displacement based bilinear softening relation is adopted, as schematically in Figure 4, further loading will cause the continuum stiffness degradation. For a particular mode, the damage variable (d_i) is introduced to produce linear softening in the stress and displacement space, from the failure initiation point δ_0^i, to complete failure δ_c^i . The notations i refer the fibre tension, fibre compression, matrix tension and matrix compression failure mode.

$$d_i = max\left\{0, min\left\{1, \frac{\delta_c^i(\delta - \delta_0^i)}{\delta(\delta_c^i - \delta_0^i)}\right\}\right\} \quad (15)$$

The displacement, δ, obtained from the strain,ε, and character element length,$l_{character}$, which alleviate strain localization problem and final results will independent of FE mesh size [35], [36]:

$$\delta = \varepsilon l_{character} \quad (16)$$

δ_0^i correspond to the critical displacement when the damage initiates, δ_c^i is the displacement at the onset of final failure obtained from the corresponding strength, $X^{C/T}$ or $Y^{C/T}$, and fracture toughness, G_i^c.

$$\delta_c^i = \frac{2G_i^c}{X^{C/T} or Y^{C/T}} \tag{17}$$

The fully-damaged element, identified by the damage variable for any of the failure modes reaching a limit of 1, was removed to avoid any instabilities.

3.2 Cohesive zone model

To evaluate the delamination or interfacial failure, the traction-separation constitutive law (bilinear elastic-linear softening model) is incorporated. It is associated with traction variables ($\sigma_n,\ \sigma_s, \sigma_t$), separation variables ($\delta_n,\ \delta_s,\ \delta_t$) and critical fracture energy release rates (G_n^c, G_s^c, G_t^c), which is controlled in a similar way as shown in Figure 4. Cohesive damage initiation was triggered by a quadratic nominal stress criterion. Cohesive damage propagation was controlled through a bilinear traction separation law based on the Benzeggagh-Kenane (BK) mixed-mode damage evolution criterion [37].

4. The material properties and numerical modelling

4.1 The T-joint FE model

The FE model of the sandwich T-joint with geometric nonlinearity effect was created using Abaqus/Explicit package. As shown in Figure 5 (a), a quarter model of the T-joint was created by taking half-length in Y-Z symmetry plane, and half-width in X-Z symmetry plane. To model the test setup as shown in Figure 3, the pulling load was applied by displacement controlled condition through web panel bolt holes in the Z direction, while the displacement in X, Y directions were constrained. Three-dimensional 8-node linear brick (C3D8R) element was used for base panel, cleats, adhesive layer and foam core model. Three-dimensional 8-node cohesive element (COH3D8) of zero thickness was used to model the interface between cleat and base panel as shown in Figure 5 (b). A summary of the material properties used in the model is presented in Table 1 taken from Ref. [1].

The cohesive element between the cleats and base panel is characterised by the penalty stiffness, failure strength and fracture energy as tabulated in Table 2 which are taken from Ref.[38].

Table 1 Material properties of MTM46/HTS unidirectional composite, plain wave cloths, adhesive and foam [1]**.**

Property	Symbol	Units	MTM46/HTS	Plain wave clothes	Filler adhesive	Foam
Longitudinal Modulus	E_x	[GPa]	128.30	139.60	2.75	0.06
Transverse Modulus	E_y	[GPa]	9.00	139.60		
Shear Modulus	G_{xy}	[GPa]	3.95	52.50	1.06	0.03
Poisson's ratio	v_{xy}	[-]	0.32	0.30	0.30	0.30

Table 2 Material properties of cohesive elements used in the adhesive layer and composite fastener.

Property	Symbol	Units	Adhesive Redux420® [38]	CFRP Interlaminar [39], [40]
Penalty Stiffness / normal direction	K_n	[MPa]	2.40×10^5	1.37×10^5
Penalty Stiffness / shear direction	K_s	[MPa]	9.20×10^4	4.93×10^4
Traction Strength / normal direction	t_n	[MPa]	10	62.30
Traction Strength / shear direction	t_s	[MPa]	15	92.30
SERR* / normal direction	G^c_n	[N/mm]	0.25	0.28
SERR* / shear direction	G^c_s	[N/mm]	0.67	0.79

*SERR: Strain Energy Release Rate or Fracture Toughness

4.2 Modelling of the composite fastener

To predict the inter- and intra-laminar delamination as observed in the experiment, each ply of the composite fastener through-thickness was modelled using a C3D8R element. Cohesive

element COH3D8 of zero thickness was used to model the 11 interface layers between the 12 plies through-thickness and 8 layers in the axial direction of the fastener as shown in Figure 5(c). Table 3 listed the material properties for the fastener model, the strength taken from Ref. [1] and fracture toughness taken from Ref. [41], [42] as they possess similar elastic stiffness and strength. The material properties of cohesive element in the composite fastener are listed in Table 2, where the inter-laminar strength and inter-laminar fracture toughness were taken from the Refs. [39], [40]. For simplicity, the profile of the composite fasteners (body, head and tail) was set identical although the test samples might have small variation due to the limited manufacture technique.

Table 3 Fracture parameters of Carbon/epoxy (MTM46/HTS) [1], [41], [42]

Property	**Symbol**	**Units**	**Value**
Long. tension Strength	X_t	[MPa]	2278
Trans. Tension Strength	Y_t	[MPa]	33.90
Long. compression Strength	X_c	[MPa]	1352
Trans. compression Strength	Y_c	[MPa]	210
Shear Strength	S	[MPa]	98.10
Fibre fracture SERR* (tension)	G^c_{1+}	[N/mm]	91.60
Fibre fracture SERR* (compression)	G^c_{1-}	[N/mm]	79.90
Matrix fracture SERR* (tension)	G^c_{2+}	[N/mm]	0.22
Matrix fracture SERR* (compression)	G^c_{2-}	[N/mm]	1.10

*SERR: Strain Energy Release Rate or Fracture Toughness

In order to simulate the fastener-hole interaction, extensive material damage model was created in the fastener contact surface and updated by element deletion. After a contact element was deleted, new element was exposed to the contact surface. In the region where cohesive and solid elements deletion was modelled, the contact pairs were identified as 'self-contact' using the general contact algorithm built-in Abaqus. Contact pairs were defined between bolt-to-laminate by implementing tangential and normal behaviour with 0.2 friction coefficient and hard pressure-overclosure contact [3]. The bonding interface between laminates and adhesive layers were modelled through the tie constraint.

5. Results and discussion

5.1 Results from experiment and simulation

FE simulation and representative measured load-displacement results of the pure bonded T-joint without fasteners (baseline) and with fastener reinforcement subjected to pulling load are shown in Figure 6. The mark 'I', 'II', 'III' and 'IV' in the figure represents critical failure points where the delamination cracking initiation, ultimate load, post-failure and final failure occurs respectively.

From the experiment of pure bonded sandwich T-joint samples (baseline), the average ultimate load measured at the bonding failure point is 22.1 kN with a standard deviation of 2.3 kN. The numerically predicted ultimate load is 23.5kN. From the experiment of the bonded sandwich T-joint reinforced by composite fasteners, the average ultimate load measured at the bonding failure point is 26.2 kN with a standard deviation 1.2 kN, which is 18.6% larger than the baseline T-joint without fasteners. The ultimate load from numerical prediction is 27.5kN. The results from both type of joints show a very good correlation between the numerical model and test data. The results also indicate that the bilinear traction separation law used in this model is acceptable for predicting the joint failure with sufficient accuracy.

From the experiment as shown in Figure 6, it is observed that the T-joint reinforced by composite fasteners has a residual strength to carry about 16% additional ultimate load with 11% extra displacement after the bonding failure. The failure load, non-linear behaviour of the load-displacement relation and the post-failure residual strength of the T-joint have also been predicted accurately by the FE analysis. From the comparison of the T-joint strength by experiment and numerical analysis as shown in Figure 7, the difference between the ultimate

load by the numerical analysis and experiment is only 5% and 6.3% for the T-joints with and without composite fasteners respectively.

5.2 Failure mechanism of the reinforced T-joint

The deformation of the joint region at the failure points 'I', 'II', 'III' and 'IV' predicted by FE simulation and observed in the experiment are shown in Figure 8. The crack was initiated from the triangular fillet region in the X-Z symmetric plane (at δ=0.7 mm) as shown in Figure 8 (a) at point 'I'.

The subsequent load-displacement exhibits a non-linear relationship. As the crack propagates, the stress was continuously redistributed in the bonding interface and fasteners. When the remaining adhesive failed to carry more load, the T-joint reached the most critical point 'II', which indicate the debonding failure at ultimate strength associated with an abrupt drop of load. Unlike the pure bonding T-joint (baseline case), the T-joint reinforced by fasteners did not fail catastrophically at the critical point 'II'. Instead, it retains a largely reduced load-carrying capacity at additional critical point 'III'. This post-failure behaviour is because of the fasteners offering residual strength in about 16% of the T-joint ultimate strength. This post-failure behaviour was observed from the experiment result as shown in Figure 8 (b) where bonding failure occurred between the cleats and base panel. Finally, the composite fastener fractured as shown in Figure 8(a) at critical point 'IV' corresponding to the final drop of load.

To calculate the force carried by the fasteners, the pulling and shear force transferred to each fastener was determined by summing the forces acting on the fastener's FE nodes connected to the adhesive layer between the cleat and base panel. The resulting pulling and shear forces of fasteners against the T-joint displacement were plotted in Figure 9. The forces of the fasteners are negligible when the load and displacement are small. As the crack propagates along the interface, shear force transferred to the fastener is much greater than pulling force. This may be caused by the increased shear stress between the cleats and base panel subjected to bending. The analysis reveals that the crack propagates in mode II dominated stress condition and the T-joint reinforcement is attributed to shear strength improvement by the fasteners. After the T-joint reached its ultimate strength at critical point II where the cleats and base panel were detached, pulling force in the fasteners increased significantly as shown in Figure 9.

Figure 10 (a) and (b) shows the failure results of the T-joint test specimens with the cleats and base panel detached and fasteners fractured mainly in shear failure along the interface. The

specimen 4 inspection shows that excessive adhesive and unevenness distribution placed between the cleats and base panel. This reduced significantly the bonding quality and strength and caused the initial crack of the T-joint [1]. The fasteners were eventually pulled out from the base panel with one of the fasteners from specimen 4 as shown in Figure 10 (c).

From the numerical simulation, the failure index contour map for the adhesive cohesive, matrix compression and delamination cohesive damage of fasteners are shown in Figure 10 (d). The simulation reveals that the composite fasteners are deformed by rotating towards the interlaminar shear loading direction and fractured in matrix compression failure mode. The fastener failure is dominated by transverse shear at an angle from the loading direction[36]. Due to the shear force in the joint interface, the centre of the fastener body was subjected to extensive contact force that resulted in crack and delamination and eventually ruptured into two pieces when the stress reached the ultimate strength.

From the test results, split fibres in the head indicated that the failure was dominated by delamination in the fastener's fillet corner due to pulling force. The fillet corner region of the fastener head subjected to bending was delaminated and predicted in the FE analysis. Since the head was formed after the composite rod was manufactured, the local material property and strength was reduced due to post-process and sparse fibres. In order to represent the characteristics in the fastener model, the CZM properties of strain energy release rate in the composite head was reduced by 50%. The results showed that the T-joint failure load was reduced to 24.9 kN. The pull-out fastener as shown in Figure 10 (c) was modelled by the fractured fastener as shown in Figure 10 (e). Although the failure details are not identical, the results provide useful data for the model validation and lead to the prediction of the T-joint failure mode.

5.3 FE analysis of T-joint reinforced by composite fasteners versus metallic opponent

In order to provide a reference case for evaluating the composite fasteners, an FE model was created for the T-joint reinforced by titanium fasteners. The material properties of the titanium alloy (Ti-6Al-4v) are listed in Table 4.

Table 4 Material properties of the titanium fastener (Ti-6Al-4v)

Young's Modulus	Shear Modulus	Poisson's ratio	Yield Strength	Density
116.0 (GPa)	43.60 (GPa)	0.33	897.0 (MPa)	4.51 (g/cm^3)

The analysis was conducted to predict the crack propagation and strength of the T-joint and in particular the fasteners. The resulting pulling load versus displacement of the T-joint reinforced by composite fasteners (CF) and titanium fasteners (TF) are compared as shown in Figure 11 together with the crack propagation at intervals of loading 8 kN, 21 kN and 27.5 kN corresponding to the point A, B and C respectively in the figure. From the simulation results, the following observations can be obtained.

The T-joints of two types of fasteners have almost the same load-deformation results until the applied load reached 21 kN at point 'B'. This indicates that the T-joint stiffness and crack initiation mainly depends on the adhesive bonding properties rather than the type of fasteners. At load point, 'A', initial crack occurred in the triangular fillet region for both type of T-joint reinforcement with the same level of damage. As the pulling load was increased to point 'B', an additional crack occurred along the edge of the cleat connected to the base panel and subsequently at the edge of the holes. The obvious difference of the load-displacement between the two types of T-joint appeared at load point 'C' where the T-joint reinforced by titanium fasteners had less cohesive element damage, higher stiffness and ultimate strength. From the numerical analysis, the failure load for the T-joint reinforced by titanium fasteners is 30.3 kN, which is 10.2% higher than that reinforced by composite ones. At the failure load point, it was also predicted that 14.2 kN shear force was transferred to the titanium fasteners comparing with 8.2 kN in the composite fasteners. In the same time, 1.5 kN and 1.2 kN axial force was transferred to the titanium and composite fasteners respectively. The results have shown again that the T-joint strength is increased mainly due to improved shear failure resistance by the fastener reinforcement.

6. Parametric study of the composite fastener

The investigation was further extended into the influence of the composite fastener's diameter and laminate layup to the T-joint strength. The resulting strength of those T-joints reinforced

by different composite fasteners in terms of shear modulus and diameters is plotted in Figure 12. The dotted line presents the results of the fastener of 5 mm diameter made of 12 plies prepreg laminate; the solid line presents the fasteners of 5.64 mm diameter with 14 plies; the double solid line presents the fasteners of 6.28 mm diameter with 16 plies. The equivalent shear modulus of the fastener was altered by varying the laminate lay-up. For example, the fastener of 6.28 mm diameter with $[(\pm 35)_4]_s$ lay-up is of shear modulus of 30 GPa. The corresponding T-joint strength was increased to 30.3 kN, which is at the same level as the T-joint reinforced by titanium fasteners. The T-joint strength can be further increased by taking lay-up $[(\pm 45)_4]_s$ for the composite fastener of increased shear modulus. In terms of weight saving, the 3.5 g mass of the composite fastener of 6.28 mm diameter is only 44% of the 6.3 g mass of titanium fastener of 5 mm diameter.

7. Conclusions

An investigation into the composite fastener made of PEEK and its application to a sandwich T-joint reinforcement has been conducted by experimental and numerical methods. The numerical model has been validated by using the experimental data to simulate the crack propagation and reveal the failure mechanism of the T-joint. Some conclusive remarks can be drawn from the investigation.

- The composite fasteners of 5mm diameter provide T-joint reinforcement with strength improvement by 18.6% compared with the bonded baseline T-joint subject to pulling load.
- Based on the FE damage model verified by experimental data, the prediction of the initial crack and propagation reveals that the T-joint failure is initially in mode II and the strength improvement mainly attributed to the fastener resistance to shear failure of the adhesive layer.
- The numerical analysis and experimental results indicate the fracture of composite fasteners at ultimate load in shear failure and eventually pull-out failure mode. The pull-out failure occurred in the fastener head is partly attributed to the pre-mature technique in the composite fastener manufacture.
- The T-joint reinforced by composite fasteners is of 10% lower strength than the titanium opponent of the same diameter due to titanium's higher shear strength.
- When increasing the composite fastener diameter to 6.24 mm and changing the laminate layup to $[(\pm 35)_4]_s$, the T-joint reinforced by composite fasteners can reach the same

strength as that reinforced by titanium fasteners of 5 mm diameter. In addition, the composite fastener has 44% weight saving compared with its titanium opponent.

Acknowledgement

The authors acknowledge the financial support from China Scholarship Council (CSC NO. 201708140099).

Reference:

[1] S. Guo and R. Morishima, "Numerical analysis and experiment of composite sandwich T-joints subjected to pulling load," *Compos. Struct.*, vol. 94, no. 1, pp. 229–238, 2011.

[2] U. Turaga and C. T. Sun, "Failure modes and load transfer in sandwich T-joints," *J. Sandw. Struct. Mater.*, vol. 2, no. 3, pp. 225–245, 2000.

[3] G. Kelly, "Quasi-static strength and fatigue life of hybrid (bonded/bolted) composite single-lap joints," *Compos. Struct.*, vol. 72, no. 1, pp. 119–129, 2006.

[4] Y. Liu, S. Lemanski, X. Zhang, D. Ayre, and H. Y. Nezhad, "A finite element study of fatigue crack propagation in single lap bonded joint with process-induced disbond," *Int. J. Adhes. Adhes.*, vol. 87, pp. 164–172, Dec. 2018.

[5] L. Zhao, Z. Fang, F. Liu, M. Shan, and J. Zhang, "A modified stiffness method considering effects of hole tensile deformation on bolt load distribution in multi-bolt composite joints," *Compos. Part B Eng.*, vol. 171, pp. 264–271, Aug. 2019.

[6] N. M. Chowdhury, W. K. Chiu, J. Wang, and P. Chang, "Experimental and finite element studies of bolted, bonded and hybrid step lap joints of thick carbon fibre/epoxy panels used in aircraft structures," *Compos. Part B Eng.*, vol. 100, pp. 68–77, Sep. 2016.

[7] F. Liu, X. Lu, L. Zhao, J. Zhang, N. Hu, and J. Xu, "An interpretation of the load distributions in highly torqued single-lap composite bolted joints with bolt-hole clearances," *Compos. Part B Eng.*, vol. 138, pp. 194–205, Apr. 2018.

[8] H. S. Li, R. J. Gu, and X. Zhao, "Global sensitivity analysis of load distribution and displacement in multi-bolt composite joints," *Compos. Part B Eng.*, vol. 116, pp. 200–

210, May 2017.

[9] E. E. Theotokoglou and T. Moan, “Experimental and numerical study of composite T-joints,” *J. Compos. Mater.*, vol. 30, no. 2, pp. 190–209, 1996.

[10] E. E. Theotokoglou, “Strength of composite T-joints under pull-out loads,” *J. Reinf. Plast. Compos.*, vol. 16, no. 6, pp. 503–518, 1997.

[11] F. Dharmawan, R. S. Thomson, H. Li, I. Herszberg, and E. Gellert, “Geometry and damage effects in a composite marine T-joint,” *Compos. Struct.*, vol. 66, no. 1–4, pp. 181–187, 2004.

[12] V. Dahmen, A. J. Redmann, J. Austermann, A. L. Quintanilla, S. J. Mecham, and T. A. Osswald, “Fabrication of hybrid composite T-joints by co-curing with 3D printed dual cure epoxy,” *Compos. Part B Eng.*, vol. 183, p. 107728, Feb. 2020.

[13] S. W. Kandebo, “Super Hornet cost reductions could boost export potential,” *Aviat. Week Space Technol.*, vol. 152, no. 15, p. 58, 2000.

[14] R. T. Cole, E. J. Bateh, and J. Potter, “Fasteners for composite structures,” *Composites*, vol. 13, no. 3, pp. 233–240, 1982.

[15] Z. Peng and X. Nie, “Galvanic corrosion property of contacts between carbon fiber cloth materials and typical metal alloys in an aggressive environment,” *Surf. Coatings Technol.*, vol. 215, pp. 85–89, 2013.

[16] Z. Liu *et al.*, “Electrochemical characteristics of a carbon fibre composite and the associated galvanic effects with aluminium alloys,” *Appl. Surf. Sci.*, vol. 314, pp. 233–240, 2014.

[17] R. Starikov and J. Schön, “Quasi-static behaviour of composite joints with countersunk composite and metal fasteners,” *Compos. Part B Eng.*, vol. 32, no. 5, pp. 401–411, 2001.

[18] R. Starikov and J. Schön, “Fatigue resistance of composite joints with countersunk composite and metal fasteners,” *Int. J. Fatigue*, vol. 24, no. 1, pp. 39–47, 2002.

[19] M. Ueda, N. Ui, and A. Ohtani, “Lightweight and anti-corrosive fiber reinforced thermoplastic rivet,” *Compos. Struct.*, vol. 188, pp. 356–362, 2018.

[20] W. Li, S. Guo, I. K. Giannopoulos, S. He, and Y. Liu, “Strength enhancement of bonded

composite laminate joints reinforced by composite Pins," *Compos. Struct.*, vol. 236, Mar. 2020.

[21] F.-X. Irisarri, F. Laurin, N. Carrere, and J.-F. Maire, "Progressive damage and failure of mechanically fastened joints in CFRP laminates–Part I: Refined finite element modelling of single-fastener joints," *Compos. Struct.*, vol. 94, no. 8, pp. 2269–2277, 2012.

[22] M. M. Shokrieh and L. B. Lessard, "Progressive fatigue damage modeling of composite materials, Part II: Material characterization and model verification," *J. Compos. Mater.*, vol. 34, no. 13, pp. 1081–1116, 2000.

[23] F.-K. Chang and K.-Y. Chang, "A progressive damage model for laminated composites containing stress concentrations," *J. Compos. Mater.*, vol. 21, no. 9, pp. 834–855, 1987.

[24] P. P. Camanho and F. L. Matthews, "A progressive damage model for mechanically fastened joints in composite laminates," *J. Compos. Mater.*, vol. 33, no. 24, pp. 2248–2280, 1999.

[25] Y. Zhou, Z. Lu, and Z. Yang, "Progressive damage analysis and strength prediction of 2D plain weave composites," *Compos. Part B Eng.*, vol. 47, pp. 220–229, 2013.

[26] X. F. Hu, A. Haris, M. Ridha, V. B. C. Tan, and T. E. Tay, "Progressive failure of bolted single-lap joints of woven fibre-reinforced composites," *Compos. Struct.*, vol. 189, pp. 443–454, 2018.

[27] M. Tarfaoui, A. El Moumen, and K. Lafdi, "Progressive damage modeling in carbon fibers/carbon nanotubes reinforced polymer composites," *Compos. Part B Eng.*, vol. 112, pp. 185–195, 2017.

[28] F. Ascione, "The influence of adhesion defects on the collapse of FRP adhesive joints," *Compos. Part B Eng.*, vol. 87, pp. 291–298, Feb. 2016.

[29] H. Cui, Y. Li, Y. Liu, J. Guo, and Q. Xu, "Numerical simulation of composites joints failure based on cohesive zone model," *Acta Mater. Compos. Sin.*, vol. 27, no. 2, pp. 161–168, 2010.

[30] H. Cui, "Simulation of ductile adhesive failure with experimentally determined cohesive law," *Compos. Part B Eng.*, vol. 92, pp. 193–201, 2016.

[31] F. Ascione, “Mechanical behaviour of FRP adhesive joints: A theoretical model,” *Compos. Part B Eng.*, vol. 40, no. 2, pp. 116–124, Mar. 2009.

[32] C. Lee, J. Kim, S. Kim, D. Ryu, and J. Lee, “Initial and progressive failure analyses for composite laminates using Puck failure criterion and damage-coupled finite element method,” *Compos. Struct.*, vol. 121, pp. 406–419, 2015.

[33] L. Jia *et al.*, “Combined modelling and experimental studies of failure in thick laminates under out-of-plane shear,” *Compos. Part B Eng.*, vol. 105, pp. 8–22, 2016.

[34] Z. Hashin, “Failure criteria for unidirectional fiber composites,” *J. Appl. Mech.*, vol. 47, no. 2, pp. 329–334, 1980.

[35] P. P. Camanho, C. G. Dávila, S. T. Pinho, L. Iannucci, and P. Robinson, “Prediction of in situ strengths and matrix cracking in composites under transverse tension and in-plane shear,” *Compos. Part A Appl. Sci. Manuf.*, vol. 37, no. 2, pp. 165–176, Feb. 2006.

[36] P. P. Camanho, A. Arteiro, A. R. Melro, G. Catalanotti, and M. Vogler, “Three-dimensional invariant-based failure criteria for fibre-reinforced composites,” *Int. J. Solids Struct.*, vol. 55, pp. 92–107, Mar. 2015.

[37] M. L. Benzeggagh and M. Kenane, “Measurement of mixed-mode delamination fracture toughness of unidirectional glass/epoxy composites with mixed-mode bending apparatus,” *Compos. Sci. Technol.*, vol. 56, no. 4, pp. 439–449, 1996.

[38] H. Cui, Y. Li, Y. Liu, J. Guo, and Q. Xu, *Numerical simulation of composites joints failure based on cohesive zone model*, vol. 27. 2010.

[39] I. Shahid and F.-K. Chang, “An accumulative damage model for tensile and shear failures of laminated composite plates,” *J. Compos. Mater.*, vol. 29, no. 7, pp. 926–981, 1995.

[40] S. T. Pinho, P. Robinson, and L. Iannucci, “Fracture toughness of the tensile and compressive fibre failure modes in laminated composites,” *Compos. Sci. Technol.*, vol. 66, no. 13, pp. 2069–2079, 2006.

[41] A. Faggiani and B. G. Falzon, “Predicting low-velocity impact damage on a stiffened composite panel,” *Compos. Part A Appl. Sci. Manuf.*, vol. 41, no. 6, pp. 737–749, 2010.

[42] A. Jumahat, C. Soutis, and A. Hodzic, "A graphical method predicting the compressive strength of toughened unidirectional composite laminates," *Appl. Compos. Mater.*, vol. 18, no. 1, pp. 65–83, 2011.

List of figures:

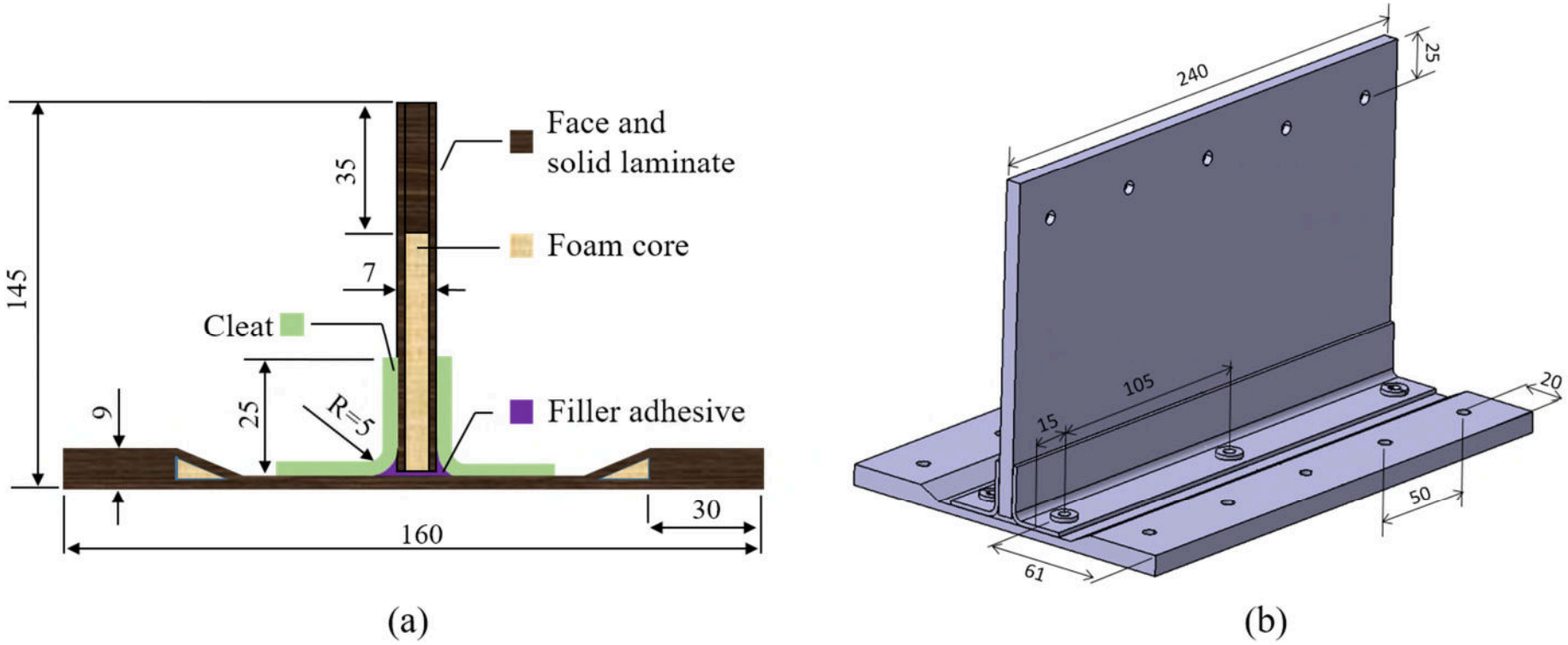
Face and
solid laminate
Foam core
Cleat
Filler adhesive
145
35
7
25
9
R=5
160
30
(a)
240
25
105
15
20
50
61
(b)

Figure 1

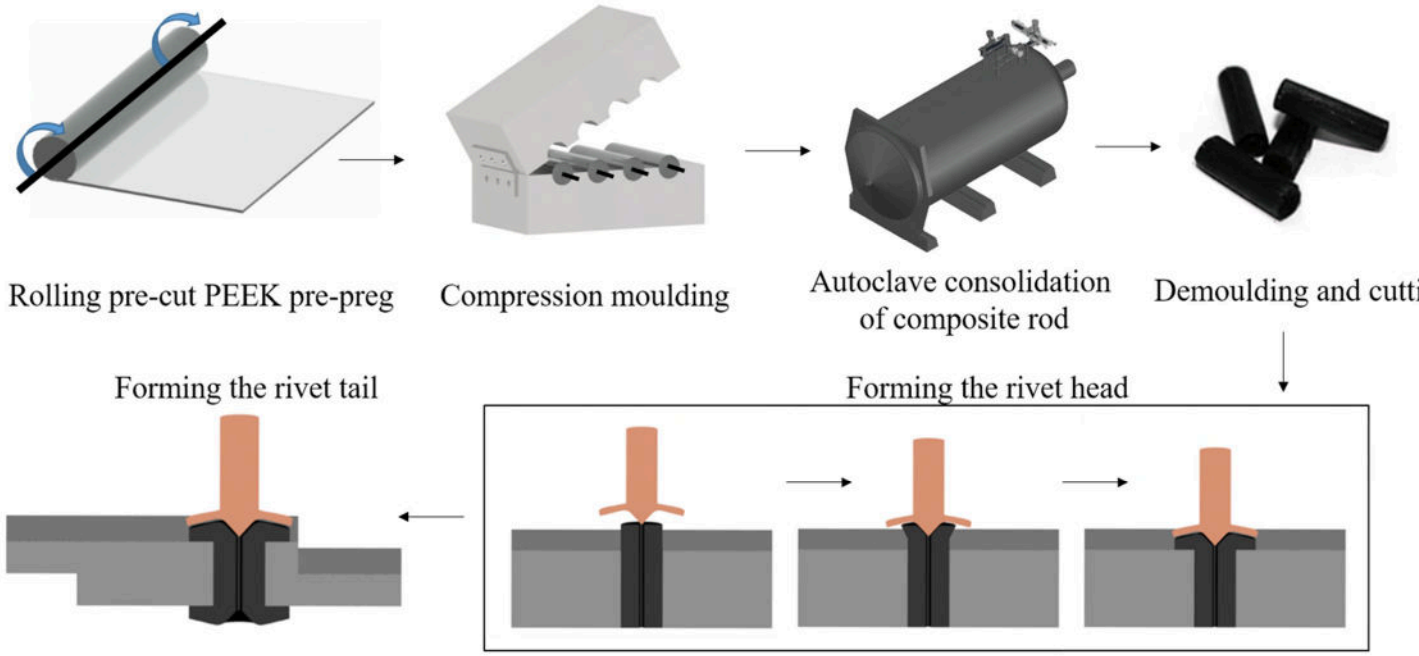

(a)

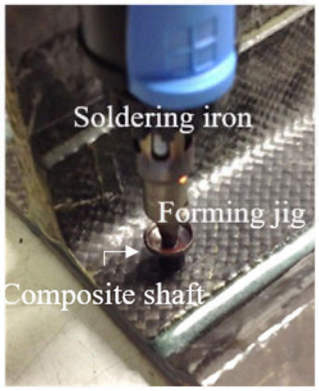

(b)

(c)

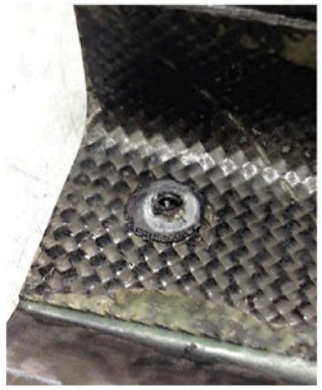

(d)

Figure 2

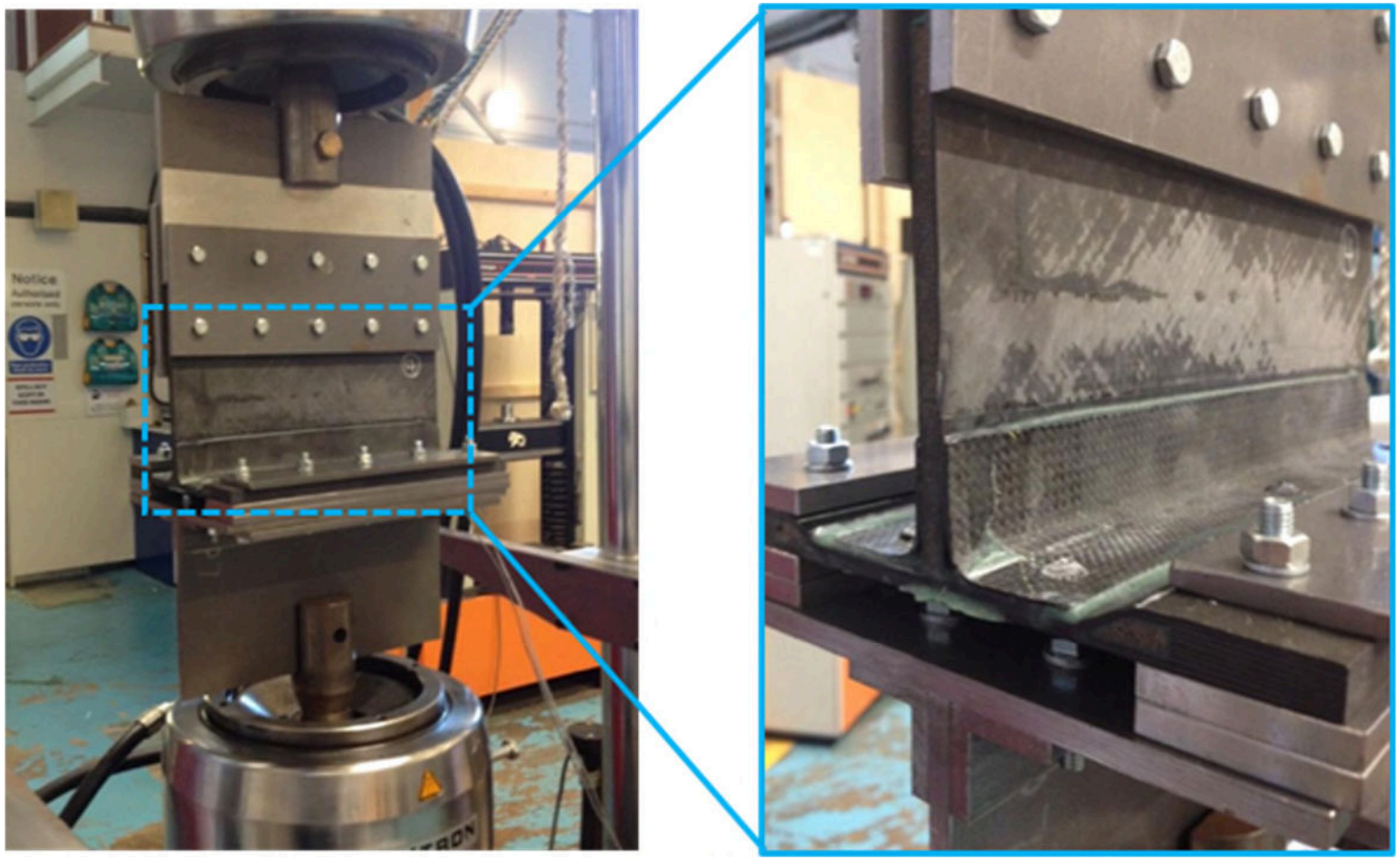

Figure 3

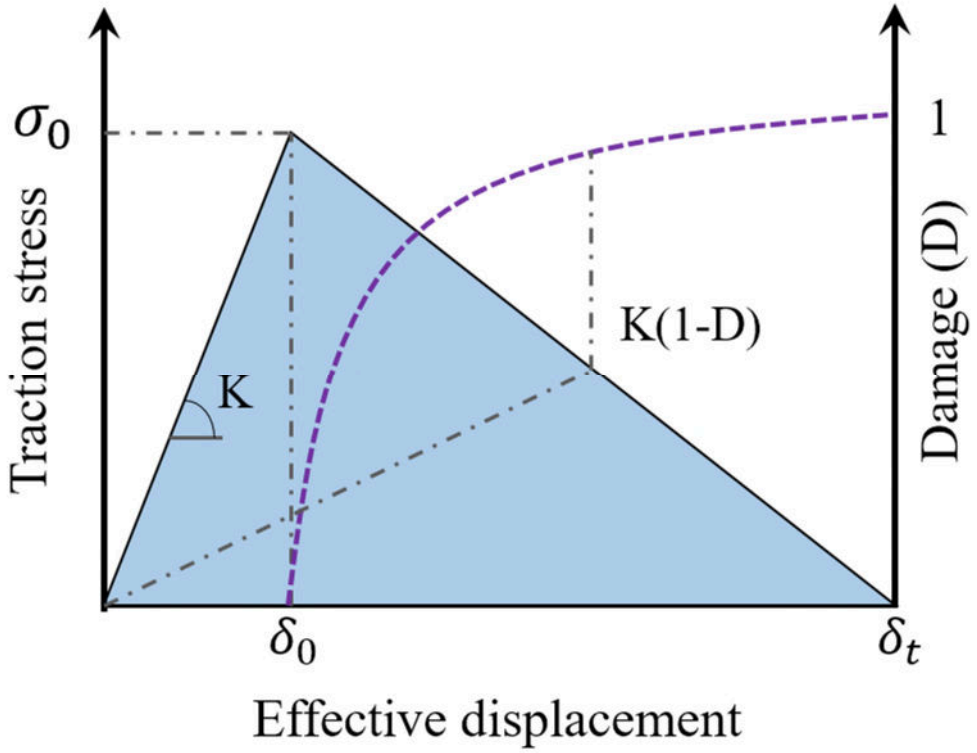
σ_0
Traction stress
K
K(1-D)
1
Damage (D)
δ_0
δ_t
Effective displacement

Figure 4

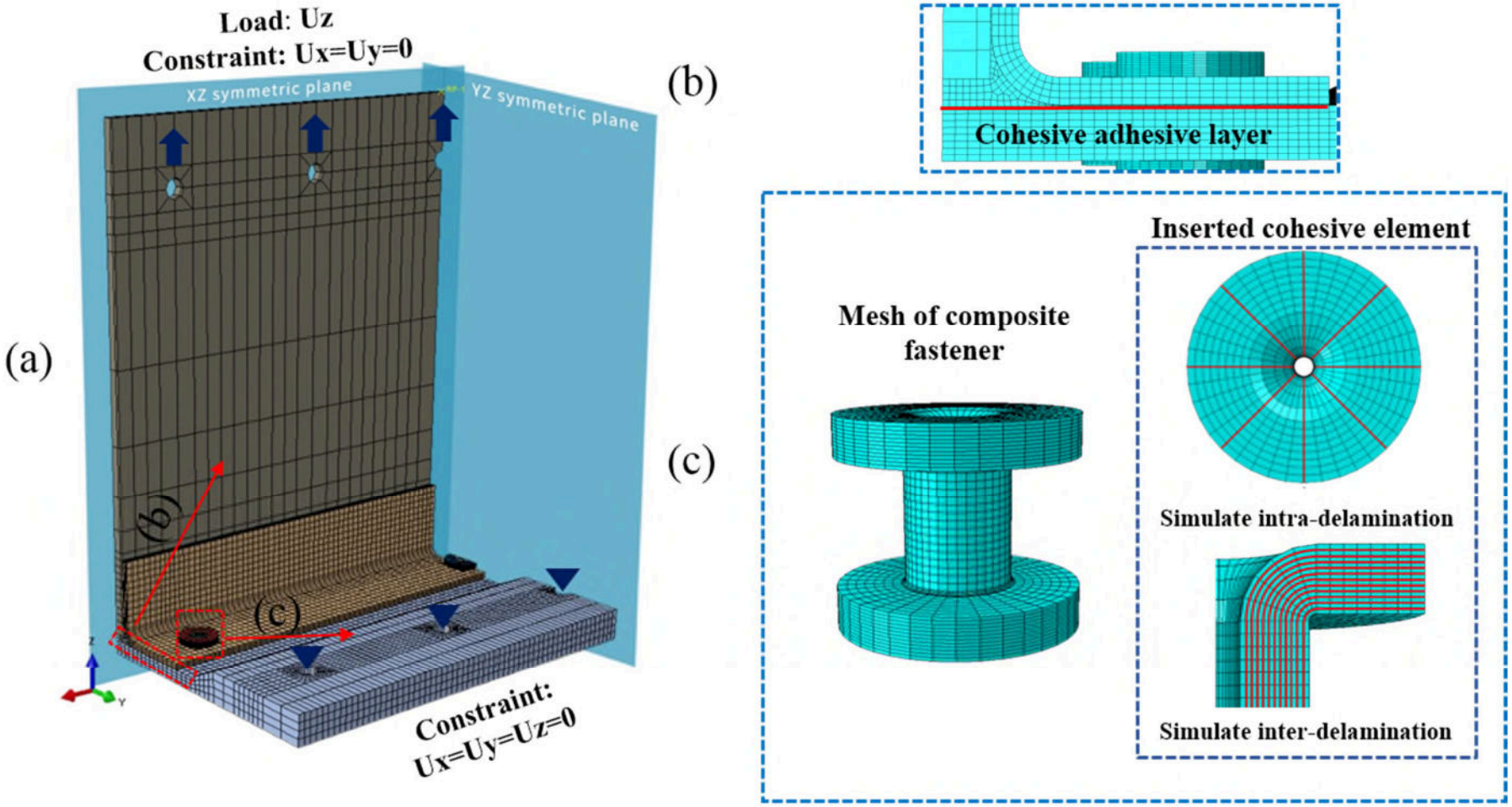
(a)
Load: Uz
Constraint: Ux=Uy=0
XZ symmetric plane
YZ symmetric plane
(b)
(c)
Constraint:
Ux=Uy=Uz=0
(b)
Cohesive adhesive layer
(c)
Mesh of composite fastener
Inserted cohesive element
Simulate intra-delamination
Simulate inter-delamination

Figure 5

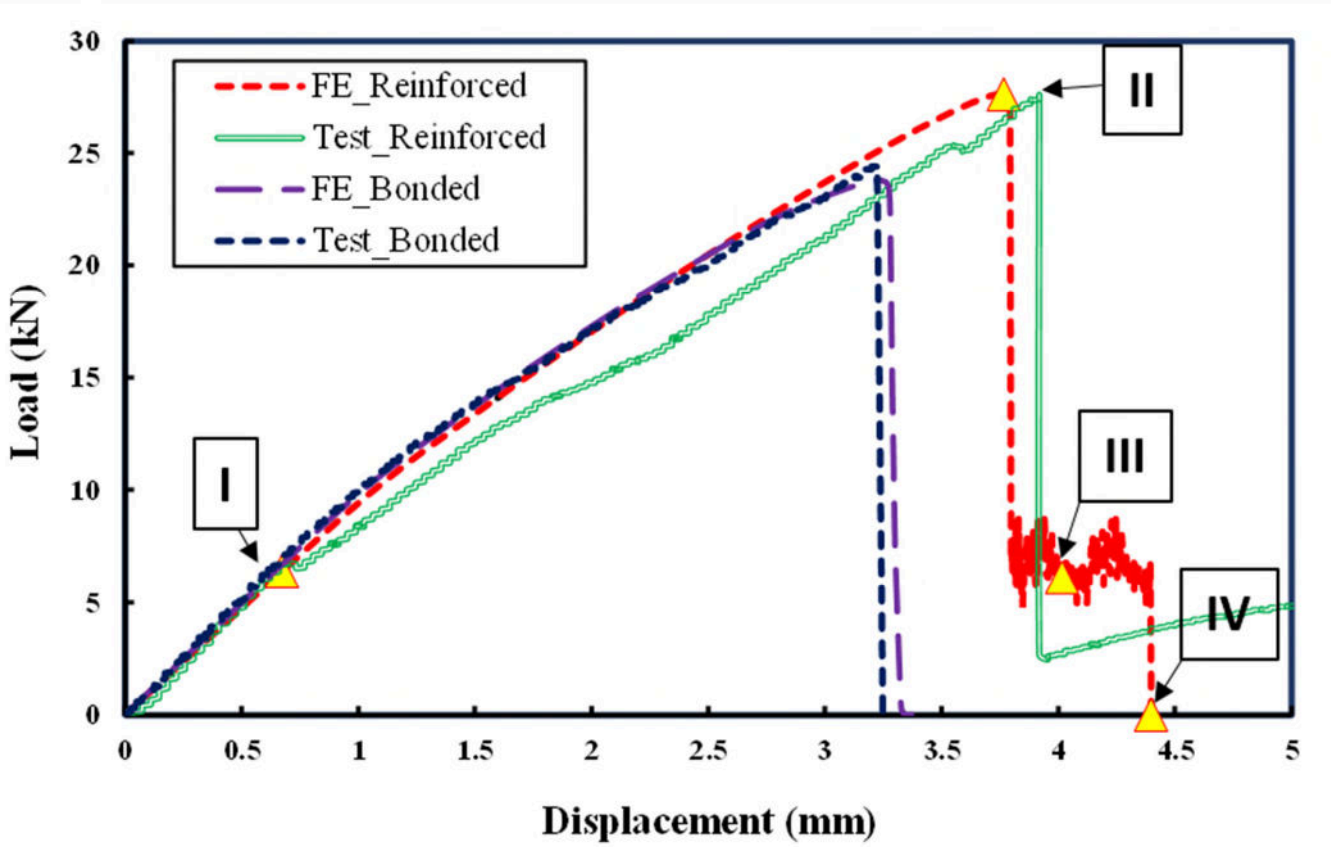
FE_Reinforced
Test_Reinforced
FE_Bonded
Test_Bonded
I
II
III
IV
Load (kN)
Displacement (mm)
0
5
10
15
20
25
30
0
0.5
1
1.5
2
2.5
3
3.5
4
4.5
5

Figure 6

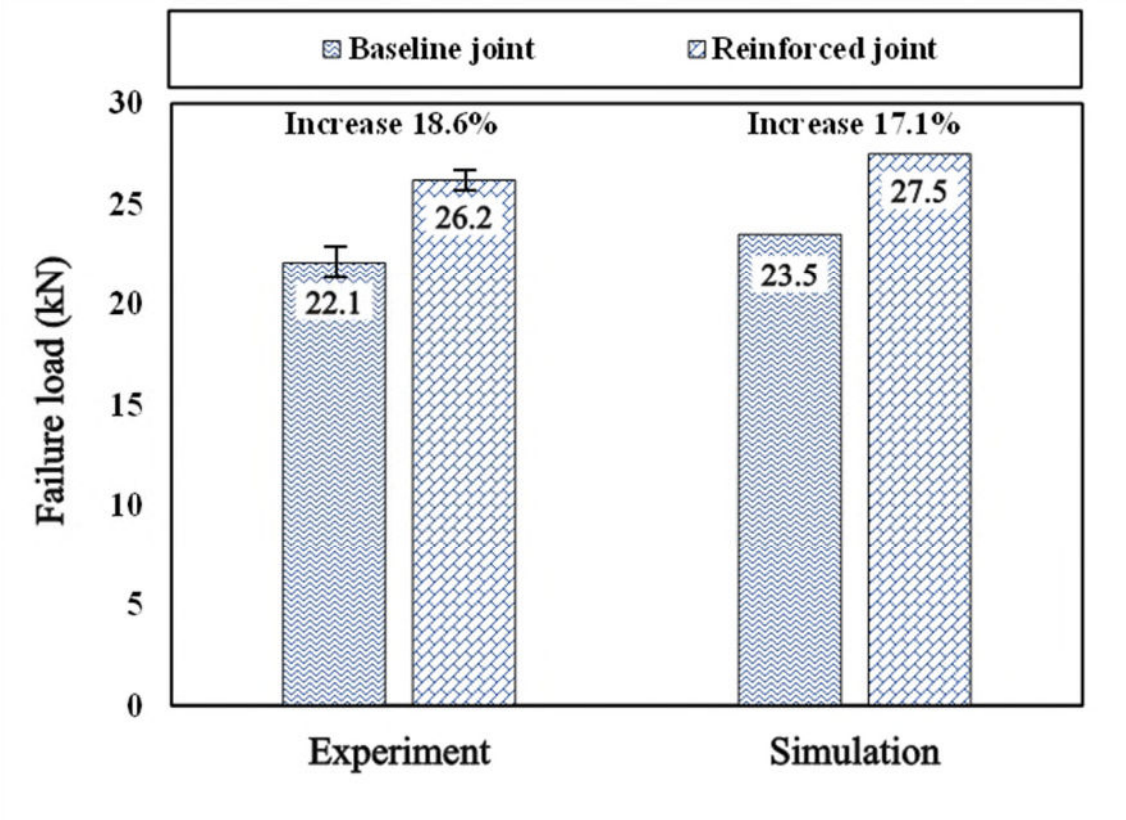
Baseline joint
Reinforced joint
Failure load (kN)
30
25
20
15
10
5
0
Increase 18.6%
Increase 17.1%
22.1
26.2
23.5
27.5
Experiment
Simulation

Figure 7

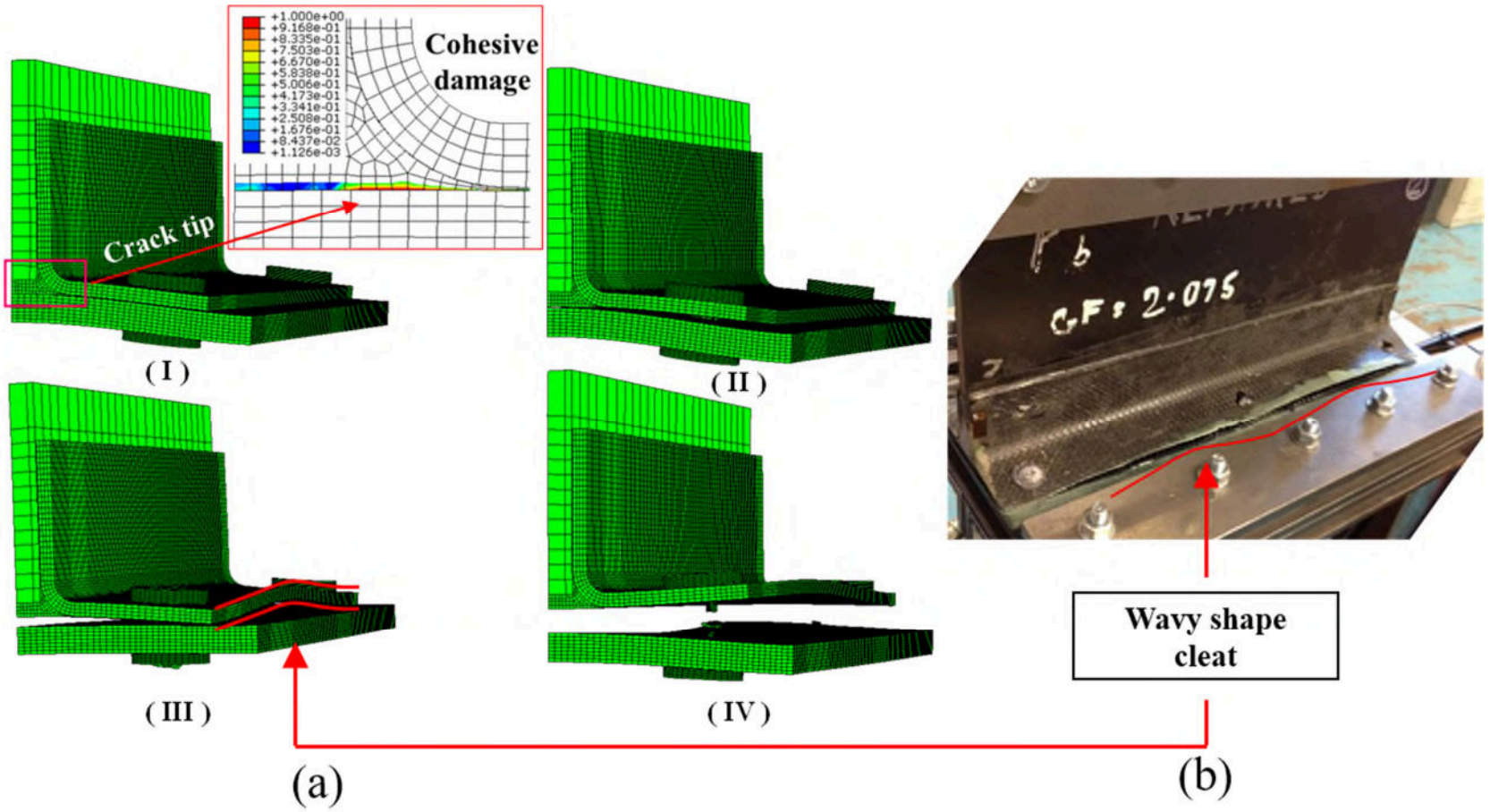
+1.000e+00
+9.168e-01
+8.335e-01
+7.503e-01
+6.670e-01
+5.838e-01
+5.006e-01
+4.173e-01
+3.341e-01
+2.508e-01
+1.676e-01
+8.437e-02
+1.126e-03
Cohesive damage
Crack tip
(I)
(II)
(III)
(IV)
Wavy shape cleat
(a)
(b)

Figure 8

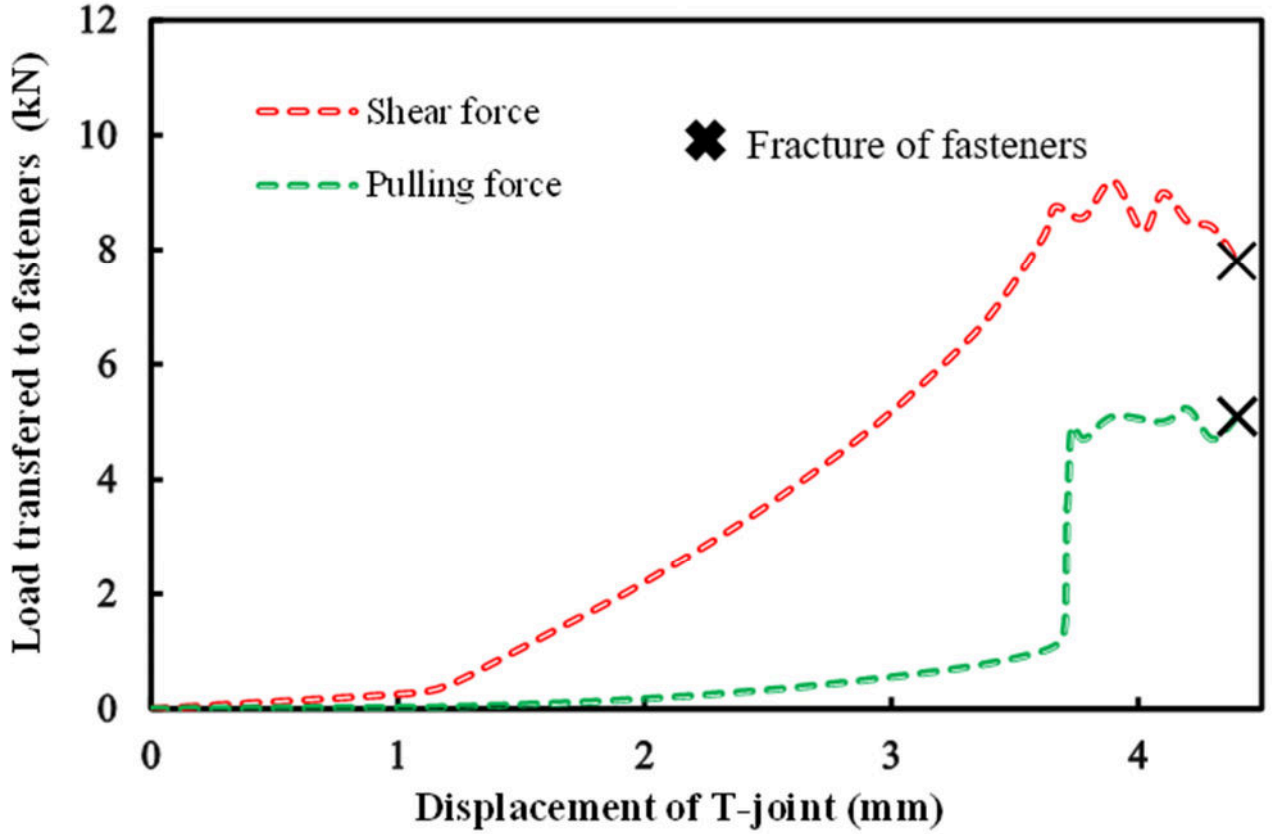
Load transfered to fasteners (kN)
12
10
8
6
4
2
0
Shear force
Pulling force
Fracture of fasteners
0
1
2
3
4
Displacement of T-joint (mm)

Figure 9

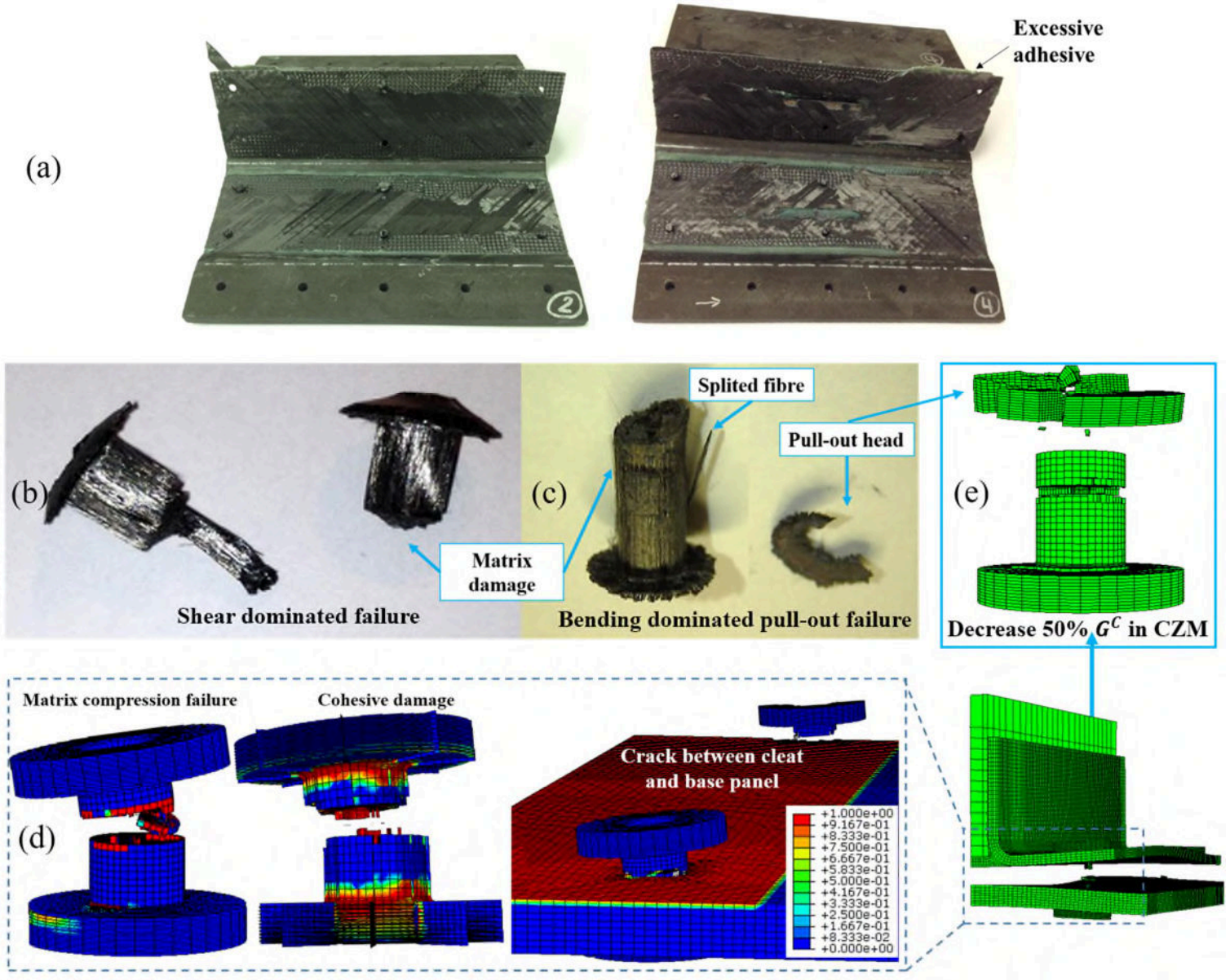
(a)
Excessive adhesive
(b)
Shear dominated failure
(c)
Splited fibre
Pull-out head
Matrix damage
Bending dominated pull-out failure
(e)
Decrease 50% G^C in CZM
(d)
Matrix compression failure
Cohesive damage
Crack between cleat and base panel
+1.000e+00
+9.167e-01
+8.333e-01
+7.500e-01
+6.667e-01
+5.833e-01
+5.000e-01
+4.167e-01
+3.333e-01
+2.500e-01
+1.667e-01
+8.333e-02
+0.000e+00

Figure 10

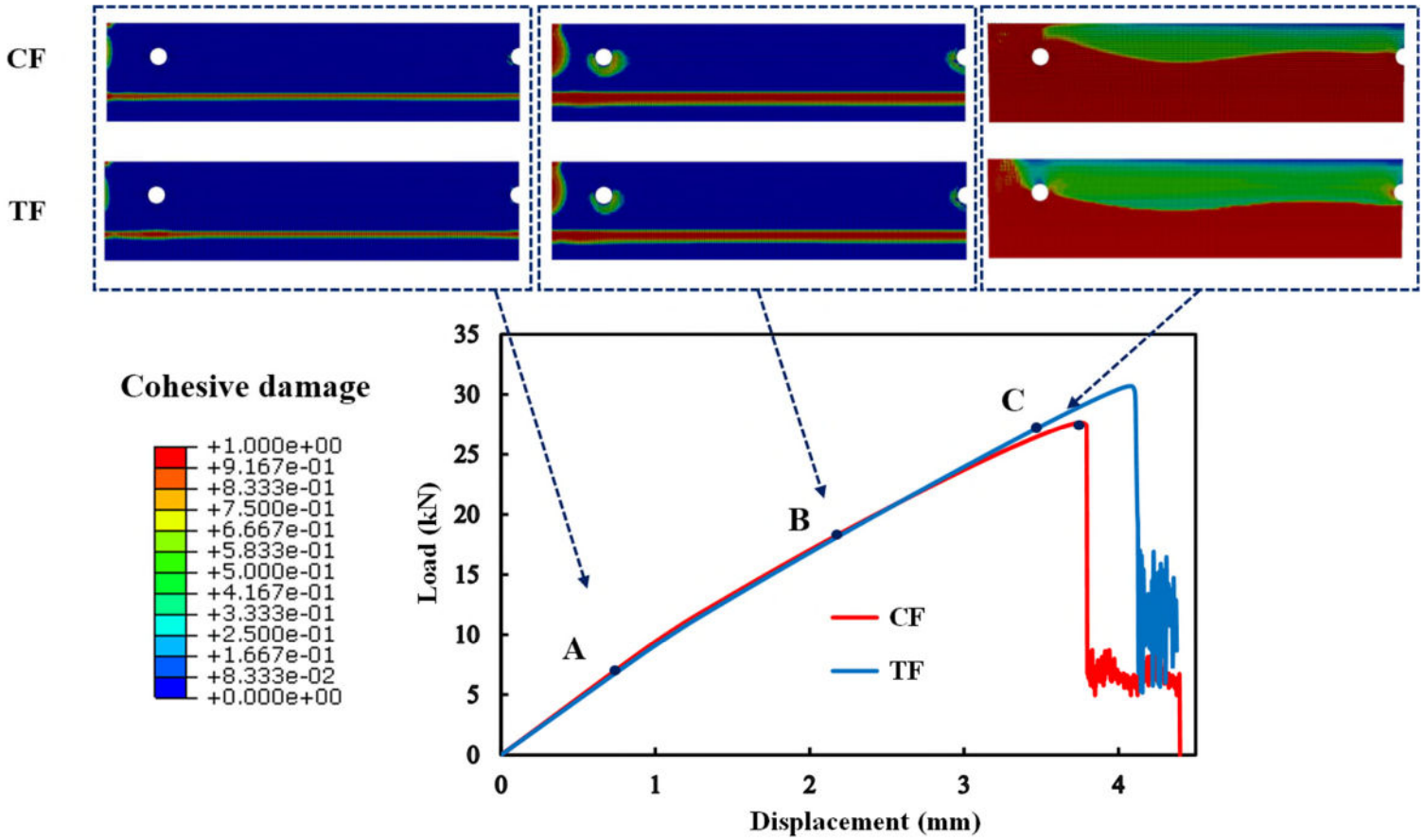
CF
TF
Cohesive damage
+1.000e+00
+9.167e-01
+8.333e-01
+7.500e-01
+6.667e-01
+5.833e-01
+5.000e-01
+4.167e-01
+3.333e-01
+2.500e-01
+1.667e-01
+8.333e-02
+0.000e+00
A
B
C
CF
TF
Load (kN)
Displacement (mm)
0
5
10
15
20
25
30
35
0
1
2
3
4

Figure 11

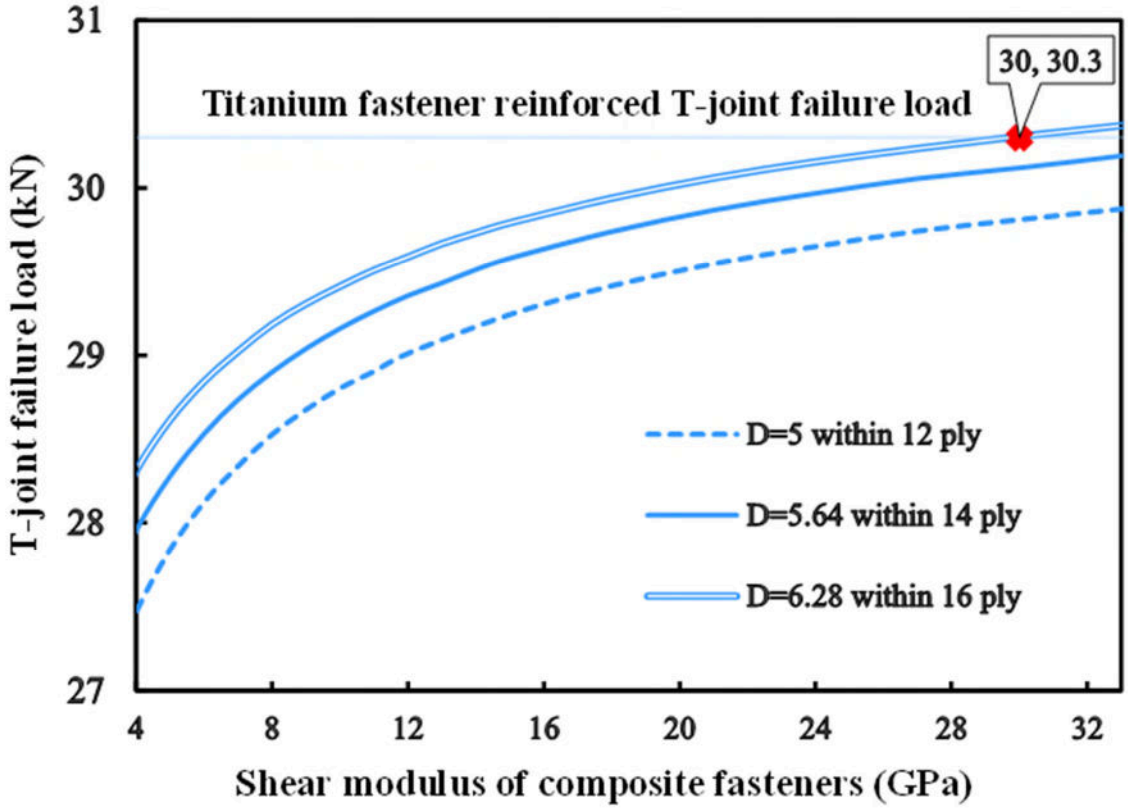
31
30
29
28
27
T-joint failure load (kN)
Titanium fastener reinforced T-joint failure load
30, 30.3
D=5 within 12 ply
D=5.64 within 14 ply
D=6.28 within 16 ply
4
8
12
16
20
24
28
32
Shear modulus of composite fasteners (GPa)

Figure 12

2020-07-29

Numerical analysis and experiment of sandwich T-joint structure reinforced by composite fasteners

Guo, Shijun

Elsevier

Guo S, Li W. (2020) Numerical analysis and experiment of sandwich T-joint structure reinforced by composite fasteners. Composites Part B: Engineering, Volume 199, October 2020, Article number 108288

https://doi.org/10.1016/j.compositesb.2020.108288